References

BERTHOU, J., LIFCHITZ, A., ARTYMIUK, P. & JOLLES, P. (1982). *Proc. R. Soc. London Ser. B.* In the press.

BLAKE, C. C. F., MAIR, G. A., NORTH, A. C. T., PHILLIPS, D. C. & SARMA, R. (1976). *Proc. R. Soc. London Ser. B*, **167**, 365–377.

BOTT, R. & SARMA, R. (1976). *J. Mol. Biol.* **106**, 1037–1046.

BUEHNER, M., LIFCHITZ, A., BALLY, R. & MORNON, J. P. (1982). *J. Mol. Biol.* **159**, 353–358.

BUERGER, M. J. (1959). *Vector Space*, pp. 239–249. New York: John Wiley.

COLMAN, P. M., DEISENHOFER, J., HUBER, R. & PALM, W. (1976). *J. Mol. Biol.* **100**, 257–282.

CRAVEN, B. M. (1975). *Computer Programs ROTRAN for the Determination of Crystal Structures which Contain Rigid Body Fragments of Known Structure.* Crystallography Department, Univ. of Pittsburgh, PA 15260, USA.

CROWTHER, R. A. (1972). *The Molecular Replacement Method*, edited by M. G. ROSSMANN, pp. 174–177. New York: Gordon and Breach.

DWIGHT, H. B. (1961). *Table of Integrals and Other Mathematical Data.* New York: MacMillan.

HACKERT, M. L., FORD, G. C. & ROSSMANN, M. G. (1973). *J. Mol. Biol.* **78**, 665–673.

HARADA, Y., LIFCHITZ, A., BERTHOU, J. & JOLLES, P. (1981). *Acta Cryst.* A**37**, 398–406.

HUBER, R. (1970). *Crystallographic Computing*, edited by F. R. AHMED, pp. 96–102. Copenhagen: Munksgaard.

JOLLES, P. & BERTHOU, J. (1972). *FEBS Lett.* **23**, 21–23.

JOYNSON, M. A., NORTH, A. C. T., SARMA, V. R., DICKERSON, R. E. & STEINRAUF, L. K. (1970). *J. Mol. Biol.* **50**, 137–142.

KITTEL, C. (1968). *Introduction to Solid State Physics.* New York: John Wiley.

LATTMAN, E. E. (1972). *Acta Cryst.* B**28**, 1065–1068.

LATTMAN, E. E. (1982). Private communication.

LATTMAN, E. E. & LOVE, W. E. (1970). *Acta Cryst.* B**26**, 1854–1857.

LIFCHITZ, A., HARADA, Y., MORRIS, F., LAURENT, A. & BERTHOU, J. (1977). Abstracts *B.* Fourth Eur. Crystallogr. Meet., Oxford. PII.12, pp. 426–427.

NIXON, P. E. & NORTH, A. C. T. (1976). *Acta Cryst.* A**32**, 320–333.

PROTHERO, J. W. & ROSSMANN, M. G. (1964). *Acta Cryst.* **17**, 768–769.

RAO, S. N., JIH, J. H. & HARTSUCK, J. A. (1980). *Acta Cryst.* A**36**, 878–884.

ROSSMANN, M. G. & BLOW, D. M. (1962). *Acta Cryst.* **15**, 24–31.

SASADA, Y. (1964). *Acta Cryst.* **17**, 611–612.

SCHMIDT, W. C. JR, GIRLING, R. L., HOUSTON, T. E., SPROUL, G. D., AMMA, E. L. & HUISMAN, T. H. J. (1977). *Acta Cryst.* B**33**, 335–343.

SHANNON, C. E. (1949). *Proc. IRE*, **37**, 10–21.

TAYLOR, C. A. (1954). *Acta Cryst.* **7**, 757–763.

TOLLIN, P., MAIN, P. & ROSSMANN, M. G. (1966). *Acta Cryst.* **20**, 404–407.

TOLLIN, P. & ROSSMANN, M. G. (1966). *Acta Cryst.* **21**, 872–876.

VAND, V. & PEPINSKY, R. (1956). *Z. Kristallogr.* **108**, 1–14.

WHITTAKER, E. T. (1915). *Proc. R. Soc. Edinburgh Sect. B*, **35**, 181–194.

Acta Cryst. (1983). A**39**, 139–148

Conditions for Direct Structure Imaging in Silicon Carbide Polytypes

BY DAVID J. SMITH AND M. A. O'KEEFE

High Resolution Electron Microscope, University of Cambridge, Free School Lane, Cambridge CB2 3RQ, England

(*Received* 23 *February* 1982; *accepted* 19 *August* 1982)

Abstract

The conditions appropriate for direct structure imaging of silicon carbide polytypes in the high-resolution electron microscope have been investigated. Weak-phase-object calculations confirm that a resolution of better than 2·5 Å is necessary before polytypic stacking sequences can be identified directly. Furthermore, resolutions closely approaching 1 Å are required to resolve projected pairs of Si–C atoms, and considerably better than 1 Å is necessary to differentiate between the two species. Extensive multi-slice calculations, based on both current and projected electron-optical characteristics, show that polytype stacking should be recognizable at 500 kV up to thicknesses of 45–75 Å, but not at 100 kV, except possibly at the 'reversed' Scherzer defocus position with extremely coherent illumination. The occurrence of Fourier images complicates recognition of the correct objective-lens defocus particularly for thin crystals of the 3*C* polytype. In thicker-crystal regions (≥100 Å), where linear image contributions are small, mutual interference between diffracted beams results generally in polytype images of apparently improved resolution and, at specific thickness and defocus values, leads to images of 3*C* resembling the 'atom-pair' configuration. The latter are then explained by consideration of the image amplitude and intensity spectra. Finally, the problems of recovering specimen structure from crystals of intermediate thickness, as well as some of the factors affecting any quantitative experimental studies, are briefly discussed.

0567-7394/83/010139-10$01.50

1. Introduction

The electron-optical conditions appropriate for obtaining structure projection images of crystalline materials in the electron microscope have become very well delineated theoretically (*e.g.* Allpress & Sanders, 1973; Bursill & Wood, 1978; O'Keefe, Buseck & Iijima, 1978). At an operating voltage of 100 kV, direct imaging of all atom *positions* in materials with small unit cells ($a_0 \leq 4$ Å) is only realistically likely in thicker regions of perfect crystals (Spence, O'Keefe & Kolar, 1977), and then with reversed contrast (atom positions white), or by using an effectively 'aberration-free' condition for those comparatively few diffracted beams which form the image (Hashimoto, Endoh, Takai, Tomioka & Yokota, 1978/79). Experimental realization of such 'structure images' has been reported in (100) and (110) gold (Hashimoto *et al.*, 1978/79) and (100), (110) and (001) silicon (Izui, Furuno, Nishida & Otsu, 1978/79). For Si (110) images it has since been shown, however, that the observed 'atomic' separation is incorrect (Krivanek & Rez, 1980; Hutchison, Anstis, Humphreys & Ourmazd, 1981) – the apparent diatomic 'dumb-bells' are actually due to second-order effects. Such images should thus not be termed structure images – the expression 'interference lattice image' seems more appropriate since this denotes that the images arise from the mutual interference of diffracted beams provided only that the incident illumination has sufficient coherence (Smith, Camps & Freeman, 1981). Finally, in the vicinity of lattice defects, image interpretation in terms of atomic positions is not possible without extensive image simulation and considerable prior knowledge of the defect (see, for example, Fields & Cowley, 1978).

An alternative approach for small-unit-cell materials is to make use of higher accelerating voltages. For operation at the optimum defocus, the maximum resolution (δ) for directly interpretable image detail is given approximately by $0{\cdot}66C_s^{1/4}\lambda^{3/4}$ where C_s is the spherical-aberration coefficient of the objective lens and λ is the electron wavelength (*e.g.* Cowley, 1975). The substantial decrease in the λ term with increasing voltage more than offsets the slow rise in the C_s term dictated by saturation of pole-piece material. The end result is that images will be obtained at voltages of at least 500 kV with resolutions of around 2 Å or better which should accurately reflect the projected structure of the observed material. Indeed, such performance levels have now been reported (Kobayashi *et al.*, 1974; Horiuchi, Matsui, Bando, Katsuta & Matsui, 1978; Cosslett *et al.*, 1979; Hirabayashi, 1980). However, as we demonstrate below, image interpretation under such high-resolution conditions *may* still remain far from straightforward. Note also that 100 kV microscopes will not attain such resolution figures unless there is some breakthrough in lens design which enables the C_s values to be significantly decreased.

We consider here the possibilities for direct structure imaging of silicon carbide at accelerating voltages of both 100 and 500 kV. It is of particular relevance that the various polytypes of silicon carbide are all based upon a framework of SiC_4 (or Si_4C) tetrahedral units which stack along the *c* axis with a layer repeat spacing of 2·518 Å (*e.g.* Verma & Krishna, 1966; Shaffer, 1969) (see Fig. 1) – this distance is considerably beyond the resolution limit for directly interpretable images in current 100 kV high-resolution electron microscopes ($\delta \sim 2{\cdot}9$ Å for $C_s = 0{\cdot}7$ mm). With judicious choice of operating conditions at 100 kV, including tilted-illumination lattice imaging, it has previously been shown to be possible (Smith, Jepps & Page, 1978) to characterize transformation structures (Jepps & Page, 1980) and interfaces between transforming polytypes (Jepps & Page, 1979) as well as to identify polytypic stacking sequences directly (Jepps, Smith & Page, 1979). However, it was recognized that the situations wherein straightforward interpretation of tilted-illumination images could be made were limited. It was therefore relevant to our interest in silicon carbide, as well as being of wider implication for the study of close-packed materials, to establish whether realistic operating conditions appropriate for the direct imaging of tetrahedral units, as well as individual atom pairs, in silicon carbide could be achieved in a high-resolution electron microscope (HREM) operated at 500 kV. Thus, computations were carried out to simulate the effect of varying specimen and microscope parameters such as crystal thickness, aberration coefficients, and objective-lens defocus. This report describes some of

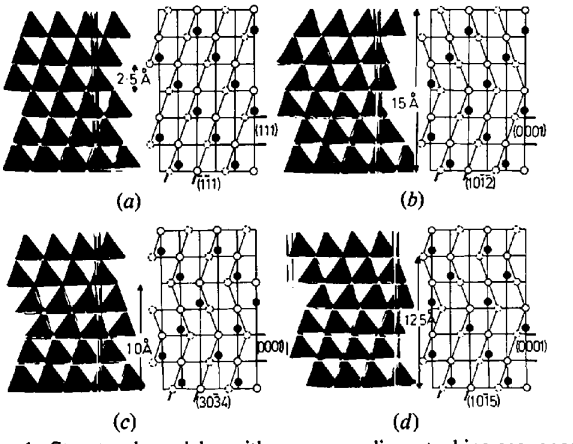

Fig. 1. Structural models, with corresponding stacking-sequence diagrams for various SiC polytypes, namely: (*a*) 3*C* viewed along $\langle 1\bar{1}0\rangle$, (*b*) 6*H* viewed along $\langle 1\bar{2}10\rangle$, (*c*) 4*H* viewed along $\langle 1\bar{2}10\rangle$, (*d*) 15*R* viewed along $\langle 1\bar{2}10\rangle$. Only those tetrahedral face planes in the zone of the viewing direction are shown on the diagrams. All the Si atomic positions are shown (those in the plane of the plan as broken circles, those above and below as closed circles), but only those C positions (filled circles) in the plane of the plan have been included (Jepps, Smith & Page, 1979).

the significant results from these simulations, as well as making the obvious comparisons with 100 kV imaging – information concerning more detailed computations is available on application to the authors. Experimental micrographs, described elsewhere, both confirm the calculations, at least for thin-crystal regions, and also highlight the necessity for careful control of the imaging conditions, particularly of crystal tilt and alignment of the incident illumination (O'Keefe, Jepps, Stobbs & Smith, 1983).

2. Simulation methods

Image simulations were performed on an IBM 370 computer using the *SHRLI* suite of programs (O'Keefe & Buseck, 1979). These are based on the Cowley–Moodie multi-slice formulation (Cowley & Moodie, 1957*a*) and permit the effects of multiple scattering, as well as specimen and instrumental parameters, to be considered. Output data from the computer were normally recorded on magnetic tape in digital form, rather than as overprinted characters on paper, since an Optronics Photo-Write was available locally to transfer this information directly onto a photographic negative. As well as being more convenient to handle in this form, the simulations appear far more realistic to the eye (since 256 grey levels are available), and are thus more easily assimilated.

3. Results

3.1. *The weak-phase-object image*

The first stage of an investigation involving computed crystal images invariably commences with simulation of the weak-phase-object (WPO) image, so-called because it represents the ideal situation wherein the effects of dynamical electron scattering within the crystal are neglected, *i.e.* the scattered beams are considered to be exactly $\pi/2$ out of phase with the central beam. This WPO image effectively provides a map of projected potential within the crystal, convolved by an aperture function to represent a sharp cut-off in spatial frequency such as might exist in a 'real' electron microscope which has perfect unit transfer of information out to the particular cut-off frequency and zero beyond it. The effect of the contrast transfer function of the objective lens in the electron microscope is, in fact, decidedly more complicated (Erikson & Klug, 1971). Nevertheless, a set of WPO images, computed for increasing values of the resolution cut-off, can be very useful as a method of comparing the resolving powers of different microscopes (O'Keefe and Pitt, 1980), although it needs to be appreciated that, because of differences in definitions of resolution, as well as envelope shapes, the WPO resolution normally has a slightly more pessimistic numerical value (typically by about 15%) than that given by δ, the directly interpretable resolution.

Conversely, a set of simulated WPO images can also serve as a useful *guide* to the microscope resolution required in order that particular features of a known specimen should become apparent. For example, we have computed a series of WPO images with increasing resolution for the 3*C* polytype projected down a (110) axis. These images show that with only five beams contributing to the image [transmitted plus 4 × (111)*s*, requiring a WPO resolution d of 2·51 Å], then the individual 'tetrahedral' sites, which can alternatively be regarded as consisting of a pair of Si and C atoms, are clearly resolved but as a rather shapeless black patch. With increasing resolution, this patch first becomes elongated ($N = 9$, $d = 1{\cdot}54$ Å), then starts to split into two separate spots ($N = 19$, $d = 1{\cdot}09$ Å) and finally becomes two clearly defined spots of different intensity ($N = 35$, $d = 0{\cdot}84$ Å), which closely resembles the projected crystal structure, with little change for further improvements in resolution.

For the polytype 6*H*, projected in the equivalent $\langle 1\bar{2}10\rangle$ direction, there is a considerable increase in the number of beams which need to contribute to the WPO images shown in Fig. 2 before these display features similar to those of 3*C* (although the corresponding cut-off resolutions are, not surprisingly, almost identical). For example, the individual tetrahedral unit

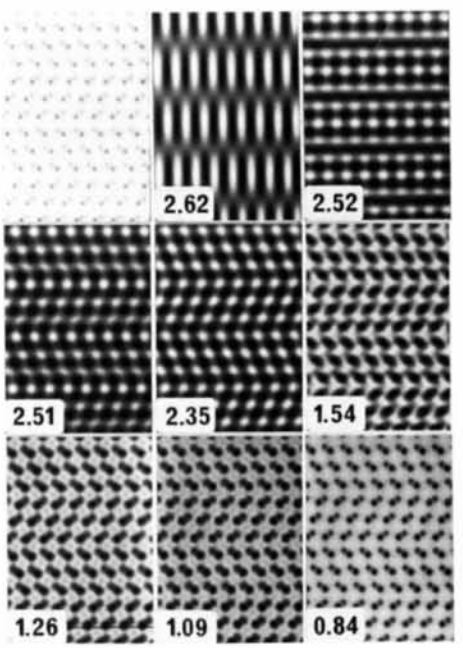

Fig. 2. Crystal structure of SiC 6*H* polytype (top left) projected along $\langle 1\bar{2}10\rangle$, together with a series of WPO images of increasing resolution, as marked (in Å).

becomes apparent for $N = 11$ ($d = 2{\cdot}51$ Å), elongation occurs for $N = 31$ ($d = 1{\cdot}54$ Å), splitting starts at about $N = 73$ ($d = 1{\cdot}09$ Å) and atoms are clearly resolved at $N = 121$ ($d = 0{\cdot}84$ Å). Moreover, it is also clear that the *C'ABCB'A'C'* tetrahedral stacking arrangement* becomes apparent for $N = 11$, *i.e.* inclusion of the four $\{10\bar{1}2\}$ diffracted beams is sufficent to identify the stacking sequence. This agrees with our previous work using tilted illumination at 100 kV (Jepps, Smith & Page, 1979) where it was found that inclusion of a $\{10\bar{1}2\}$ diffracted beam from 6*H* was necessary in order that its stacking sequence be revealed (in this case, however, information concerning tetrahedral *positions* was not provided).

Image computations (not shown) confirm that similar resolution figures also hold for the rhombohedral polytypes, such as 15*R* and 21*R* where there are no tetrahedral-face reflections such as occur for 3*C* and some hexagonal polytypes other than 4*H*.

These WPO images of the various polytypes thus of the stacking sequences under normal axial-illumination conditions necessitates a WPO resolution of slightly better than 2·5 Å. Moreover, the possibility of separately identifying the constituent C and Si atoms, rather than simply the tetrahedral sites, by means of different intensity levels, requires a WPO resolution of considerably better than 1 Å. Whilst the former figure has already been achieved in several high-voltage HREM's, the latter does not seem likely in the foreseeable future.

3.2. *Multi-slice calculations*

It is now possible to characterize accurately the instrumental parameters C_s, α and Δ in any HREM (where α is the semi-angle of the incident illumination, and Δ is the r.m.s. focal spread) by simulating images of well known test objects, such as the complex inorganic oxide $Ti_2Nb_{10}O_{29}$. Image matching with experiment is facilitated by rapid changes in appearance with defocus and thickness variations (O'Keefe, Buseck & Iijima, 1978; Wilson, 1980). The known values of these instrumental parameters can then be used in subsequent image simulations for other materials recorded under very similar operating conditions.

3.2.1. *Thickness dependence*

(*a*) 500 kV. In the particular case of the Cambridge University 600 kV HREM, for which $\delta \sim 2{\cdot}0$ Å, the values of C_s, α and Δ were previously found to be typically in the region of 3·5 mm, 0·3 mrad and 250 Å respectively for operation at an accelerating voltage of 500 kV (Wilson, Spargo & Smith, 1982). Fig. 3 shows the corresponding simulated images, for the optimum Scherzer defocus ($\Delta f_0 = \sim -700$ Å), of the polytypes 3*C*, 6*H* and 21*R* for thicknesses of 15·3 and 123 Å (slice thickness of 3·07 Å; 5 and 40 slices respectively) under axial-illumination conditions. Clearly, when the crystals are very thin (*i.e.* linear imaging conditions prevail), the individual tetrahedral sites are well resolved (*a*, *c* and *e*) with black spots representing atom pairs, the stacking sequences are easily discerned, and it would appear that any particular polytype should be readily identified directly from its image at this thickness. Equally apparent, however, is that for comparatively moderate crystal thicknesses, the large non-linear image contributions produce images in which the tetrahedral sites and the stacking sequence are no longer intuitively obvious at the Scherzer defocus (*b*, *d* and *f*). Further aspects of image resolution and interpretability, particularly for increasing crystal thickness, are discussed in more detail below (§ 3.3).

(*b*) 100 kV. It is relevant then to compare the above 500 kV simulations with those expected under normal operating conditions from high-resolution instruments having $\delta > 2{\cdot}5$ Å, *e.g.* a high-performance 100 kV microscope having C_s, α and Δ of 0·7 mm, 1 mrad and 100 Å respectively. Since the corresponding δ is larger than the tetrahedral repeat distance of 2·51 Å, the linear contribution to the image will be negligible at Scherzer focus (O'Keefe, 1979), *i.e.* the image will be

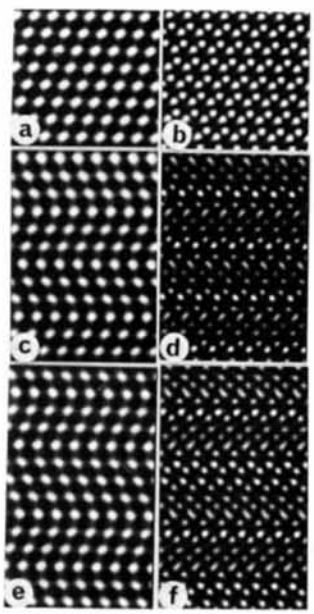

Fig. 3 Simulated 500 kV images at Scherzer defocus, for 3*C* (top row), 6*H* (middle) and 21*R* (bottom) for thicknesses of 15·3 Å (left column) and 123 Å (right column). Atom pairs are represented by black spots on the left, but are not visible on the right. $C_s = 3{\cdot}5$ mm; $\alpha = 0{\cdot}3$ mrad; $\Delta = 250$ Å.

* As noted previously, it is convenient to use a modified form of the *ABC*... notation to represent the structure of an SiC polytype, with the prime denoting a π rotation of the particular tetrahedral unit (Smith, Jepps & Page, 1978).

formed largely from second-order interferences. The contrast of the image will not be proportional to a projection of the crystal potential and hence the image will *not* be a structure image. Note, however, that for increasing crystal thicknesses the changing values of diffracted-beam amplitudes and phases may occasionally produce images bearing a 'fortuitous' resemblance to the projected structure.

An increasing thickness series at the Scherzer defocus for the 3*C* polytype is shown in Fig. 4. Clearly, it is not until thicknesses in the region of 108 Å (*i.e.* 35 slices) that the image even starts to resemble the crystal structure, although with white spots at the tetrahedral positions; these spots become elongated to correspond *roughly* to C and Si positions at around 138 Å (45 slices). A further displaced mesh of white spots appears at thicknesses in the region of 220 Å (70–75 slices). Simulations for increasing thicknesses up to 600 Å indicate that similar images will recur. Furthermore, apparent 'dumb-bell' images occur at thicknesses of about 340 Å (110 slices) and 400 Å (130 slices) – only in the latter case do these appear in the same region of the unit cell as do the atoms. Further computations for other defocus values also show that similar meshes can be obtained both at and away from the tetrahedral-site positions – 'dumb-bell' images are also sometimes found.

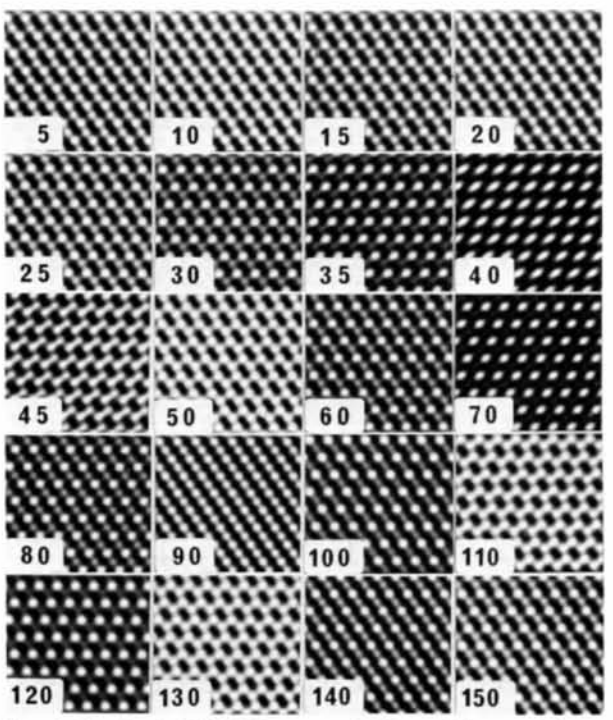

Fig. 4. Simulated 100 kV images of 3*C*, at Scherzer defocus, showing the effect of increasing crystal thickness; the slice number is marked (1 slice ≡ 3·07 Å). $C_s = 0{\cdot}7$ mm; $\alpha = 1$ mrad, $\Delta = 100$ Å.

These images suggest the possibility that stacking sequences might be recognizable, at least at certain thicknesses and defoci, despite the value of δ exceeding the layer-repeat distance of 2·51 Å. However, corresponding simulations of the 6*H* polytype indicate that this is not likely in any larger-unit-cell polytype where diffracted beams occur over a range of spatial frequencies in reciprocal space. At no thickness up to 100 slices (307 Å) is an image obtained from 6*H* which faithfully reveals the tetrahedral stacking arrangement – only the $7\frac{1}{2}$ Å half-unit-cell repeat spacing is apparent. Also note that no 'dumb-bell'-type images are observed.

Finally, it is significant that the prospects for image interpretability at the optimum focus position for an accelerating voltage of 100 kV are not improved even under what are extreme operating conditions for current microscopes. This is shown in Figs. 5(*a*) and 5(*b*) for thicknesses of ~30 and ~90 Å where values for C_s, α and Δ are taken to be 0·7 mm, 0·2 mrad and 50 Å. Note, however, that a 'zigzag' mesh pattern resembling the 6*H* structure is expected at a defocus of about −1400 Å (the 'reversed Scherzer' defocus) (Fig. 5*c*). Comparison with the model structure and the WPO image (Fig. 2) indicates that the mesh has the form of a structure image with a resolution between 2·35 and 2·51 Å, although of reversed contrast with white spots at the positions corresponding to an SiC atom pair. This mesh is no longer apparent at a thickness of ~90 Å (Fig. 5*d*). It is appropriate here also to point out that, in the presence of stacking disorder, or a lattice defect, it is unlikely that a reversed-contrast image, whose appearance can be so conveniently interpreted, will occur.

3.2.2. *Focus dependence* – 500 kV

The interpretation of high-resolution electron micrographs from small-unit-cell materials is complicated

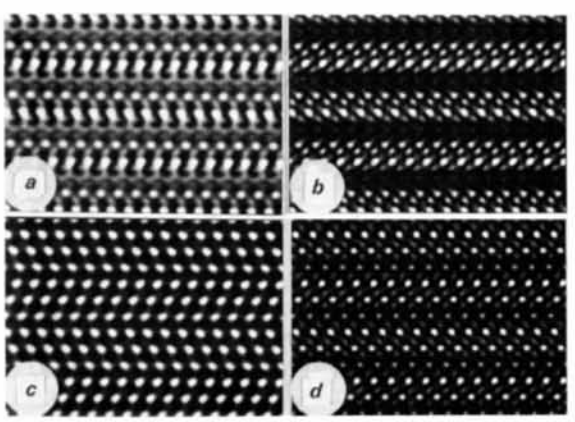

Fig. 5. Simulated images of 6*H* at 100 kV; (*a*) Scherzer defocus, 30 Å thick; (*b*) Scherzer defocus, 90 Å thick; (*c*) −1400 Å defocus, 30 Å thick; (*d*) −1400 Å thick.

considerably by the periodic recurrence with defocus of 'Fourier' or self-images of the crystal lattice (Cowley & Moodie, 1957*b*; Iijima & O'Keefe, 1979). For a simple unit cell of square side d then the Fourier image period is given by $2d^2/\lambda$ whilst, for the more general case, the Fourier period is a multiple of the separate periods of all the spacings present in the image. The thin-crystal image of 3*C* at 500 kV contains contributions from beams of both 2·17 and 2·51 Å spacing, corresponding to the 200 and 111 reflections. This gives defocus periods of 666 and 888 Å respectively, with a common period of 2664 Å. However, comparisons of the Scherzer image with the WPO images of 2·51 and 2·17 Å indicate that the 200 contribution is relatively small, at least for thin crystals, so that the Scherzer image might appear to recur at intervals of about 890 Å.

Our through-focus simulations confirm these predictions. Figs. 6(*a*) and 6(*b*) show images for a crystal of 3*C* with thicknesses of 30·7 and 153 Å respectively. For the thinner crystal, an image resembling the Scherzer image (~−800 Å) recurs both near ~+200 and ~−1700 Å, with shifted images near ~−300 and ~−1200 Å. Close examination shows, however, that there are subtle differences in appearance, presumably because of the slight influence of the 200 beams. For the thicker crystal, the situation is complicated further by the strength of the second-order image contributions. There is qualitative image matching at ~−1700 Å, although displaced, but not at ~+200 Å.

For the larger-unit-cell polytypes, such as 6*H*, an exact recurrence with defocus might not reasonably be expected because of the wide range of spatial periodicities contributing to the image. However, for thin crystals, where the image basically consists of 2·518 Å spacings, corresponding to the $\{10\bar{1}2\}$ reflections, images displaced from the Scherzer defocus by ~900 Å (*i.e.* the periodicity of the 2·518 Å spacing) are, qualitatively at least, similar to the optimum defocus image. For thicker crystals, the agreement at these same defocus values is considerably worse (see Fig. 7), as might be anticipated given that multiple scattering again increases the contributions to the image of beams with different spacing. Experimentally, recognition of the 'correct' defocus condition for direct image interpretability, particularly for thin crystals, is obviously a problem: an alternative criterion, such as the characteristics of the Fresnel fringe at the crystal edge (Wilson, Bursill & Spargo, 1978/79) is required.

Calculations have also been carried out for two of the polytypes where no tetrahedral-face reflections occur, namely 15*R* and 21*R*. These simulations display the same sort of behaviour already seen for the 3*C* and 6*H* polytypes, namely: recognizable tetrahedral-site positions at the Scherzer defocus for crystal thicknesses up to about 45 Å; periodic recurrence of qualitatively similar images with defocus, and increasing dynamical interactions with thickness which render the images uninterpretable directly. As found for the 6*H* images shown in Fig. 7, the unit-cell repeat

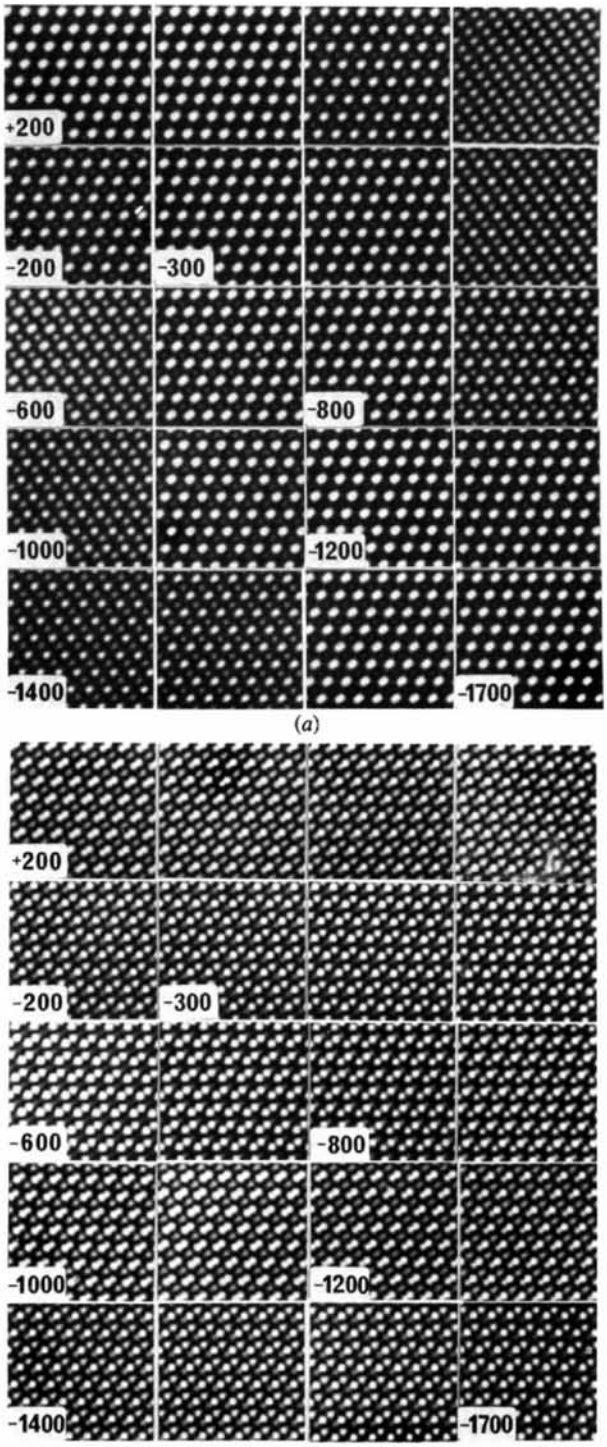

Fig. 6. Through-focal series of 3*C* images at 500 kV; 100 Å steps; some defocus values marked. (*a*) 30·7 Å thick; (*b*) 153 Å thick. C_s = 3·5 mm; α = 0·3 mrad; Δ = 250 Å; aperture cut-off 2·0 Å.

distances of 12·6 and 17·6 Å are clearly recognizable in the computed images of 15*R* and 21*R* respectively in thicker-crystal regions.

Finally, it seems appropriate to examine here whether improved, but *technically feasible*, electron-optical characteristics at 500 kV might enhance image interpretability, especially for thicker-crystal regions. Fig. 8, for example, shows simulations for increasing crystal thickness at the Scherzer defocus (here −500 Å) for both (*a*) 3*C* and (*b*) 6*H* for values of C_s and Δ of 2 mm and 150 Å respectively ($\delta \sim 1{\cdot}84$ Å). Matching with corresponding WPO simulation series (*cf.* Fig. 2 for 6*H*) indicates that the WPO resolution has improved to better than 2·17 Å for crystal thicknesses up to about 45 Å (15 slices). Moreover, direct image interpretability in terms of recognition of tetrahedral sites is perhaps possible up to thicknesses of around 75 Å (25 slices) whereas, for the previous simulations, where C_s and Δ were respectively 3·5 mm and 250 Å, comparable interpretable images were obtainable up to perhaps 45 Å. However, for thicker-crystal regions of both 3*C* and 6*H*, there are complex image variations and the problems of non-intuitive image appearance clearly remain serious, even with the better microscope parameters.

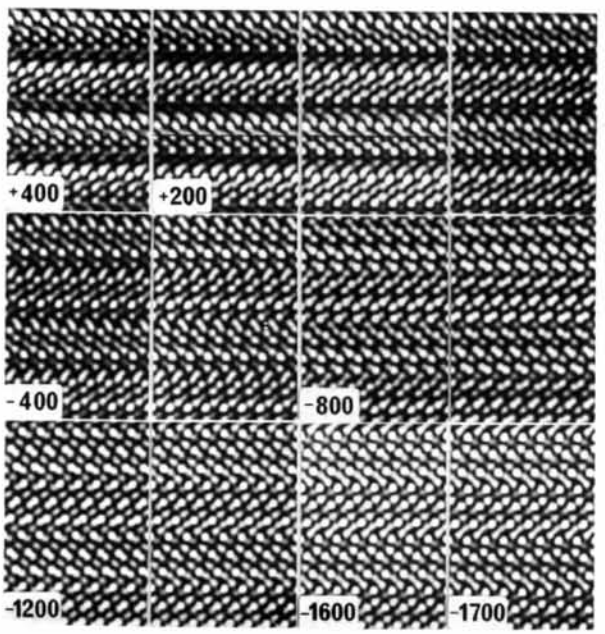

Fig. 7. Through-focal series of 6*H* images at 500 kV; 200 Å steps unless marked; 153 Å thick; C_s = 3·5 mm; α = 0·3 mrad; Δ = 250 Å.

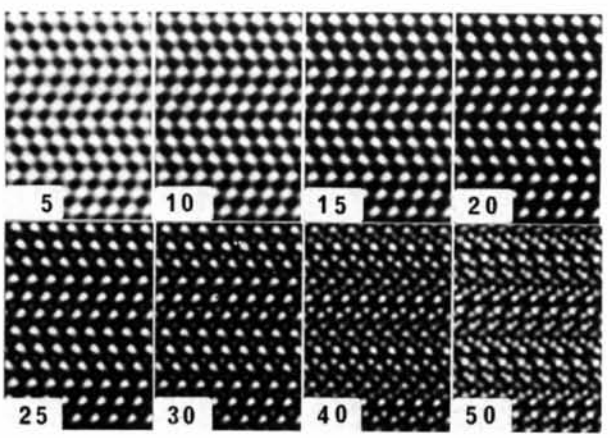

Fig. 8. Simulated 500 kV 6*H* images for increasing thickness, with improved electron-optical characteristics; slice number marked. C_s = 2·0 mm; α = 0·3 mrad; Δ = 150 Å.

3.3. *Image 'resolution' and thick crystals*

The multi-slice simulations at both 100 and 500 kV have suggested that images from thicker SiC crystal regions ($\gtrsim$100 Å) contain details considerably finer than the apparent resolution limits. A further examination of the image amplitude and intensity spectra at 500 kV, for the simple case of the 3*C* polytype, establishes that these details arise from higher-order interference terms as the unscattered beam drops away in intensity. Fig. 9(*a*), for reference, gives the amplitudes of various diffracted beams as a function of crystal thickness. As these amplitudes rise, mutual interference can produce an intensity spectrum (*i.e.* the Fourier transform of the image intensity) with some terms of magnitude comparable to, and exceeding, those of the [000–*hkl*] terms, depending on the crystal thickness and objective-lens defocus. Fig. 9(*b*) shows the relative magnitudes of several terms at a defocus of −1100 Å, when *only* seven diffracted beams (000, 111*s* and 200*s*) are used to form the image. Some of these terms correspond to the spacings of beams contributing to the thin-crystal image whilst others span larger distances in reciprocal space leading to the finer spacings seen in images from thicker crystals. In particular, when the ratios of the amplitudes of the interference terms approach those of the structure factors, 'dumb-bell' images may result.

The presence of these interference terms is a necessary pre-requisite for production of 'dumb-bell' images *whenever* the interpretable resolution is insufficient to produce them directly in thin-crystal regions. Krivanek & Rez (1980) have already shown at 100 kV, for example, that [311]-type terms in silicon projected down (110) lead to dumb-bells, though of incorrect spacing. They also demonstrated experimentally that the inclusion of [400]-type beams in CdTe images, again in (110) but with tilted illumination, provides dumb-bells with spacings correctly mimicking the projected atom positions. Similar qualitative conclusions can also be reached with 3*C* silicon carbide. Fig. 10 shows the effect of exclusion of the (200) beams from the imaging process at 500 kV, for example by choosing an objective aperture corresponding to $(2{\cdot}5\ \text{Å})^{-1}$. Comparison of Fig. 10 with the two matching series which

include the (200) beams (see Fig. 6) shows that the former contain much less detail. In the thin crystal, there is no tapering of the white 'lozenges' at the Scherzer defocus and no faint intermediate white spots occur; with the thicker crystal, no dumb-bell shapes appear. These results thus provide further confirmation that the (200) beams make significant contributions to the images.

The occurrence of white dumb-bells near the atom positions at some crystal thicknesses and lens defoci highlights the difficulty of deciding on image 'resolution' with thicker crystals. For example, the dumb-bell image from a crystal of 150 Å thickness, at −1100 Å defocus (see Fig. 6*b*), when compared with the 3*C* WPO image series is very similar to a reversed-contrast structure image with resolution between 1·31 and 1·09 Å, even though it is formed from only (111) and (200) beams which correspond to spacings of 2·51 and 2·17 Å. Strictly speaking, the dumb-bell image contains no information about the crystal beyond the 2·17 Å limit, and, since an image should not really be said to have a resolution exceeding that due to the diffracted beam of highest spatial frequency contributing to it, then this figure should be taken here as the limit of resolution. It should be appreciated, however, that although an image from a thick crystal may have an amplitude spectrum containing only low-order diffracted beams, electrons from higher orders (*i.e.* carrying high-resolution information) may have been diffracted into these beams by multiple scattering. It should also be noted that non-linear images may in some circumstances, such as the presence of considerable chromatic aberration, have a higher resolution than that of equivalent thin-crystal images: linear interferences may be damped sufficiently to make their contribution to the (thin-crystal) image negligible whereas the non-linear interferences are much less affected (*e.g.* Fig. 4).

Whilst much of the above discussion, particularly that concerning the presence of 'dumb-bells' in 3*C*, is not applicable to other silicon carbide polytypes, it also serves to highlight the general problem of establishing 'resolution' criteria (Wilson *et al.*, 1982). The finer spacings present in thicker-crystal regions clearly do not generally reflect those primary beams contributing to the image, *i.e.* those admitted by the objective aperture. Any detailed interpretation of images, par-

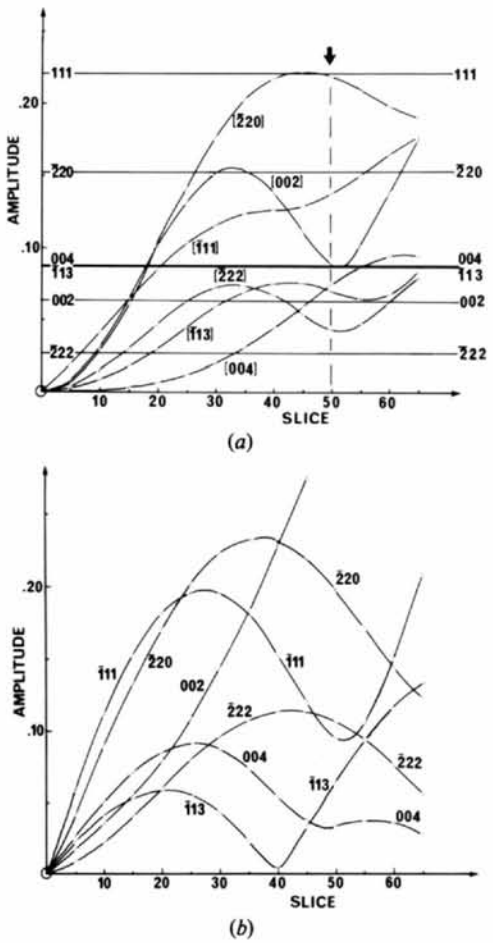

Fig. 9. (*a*) Amplitudes of diffracted beams at the crystal exit surface, as a function of thickness, for 3*C* silicon carbide at 500 kV. (Slice ≡ 3·07 Å.) (*b*) Amplitudes, as a function of thickness, of all interference terms contributing to the image for 3*C* at 500 kV with C_s = 3·5 mm; Δ = 250 Å; α = 0·3 mrad; defocus ε = −1100 Å. Note that 'dumb-bell'-type images occur when the ratios of the amplitudes of most of the interference terms approach those of the structure amplitudes (horizontal lines) – one such position is arrowed.

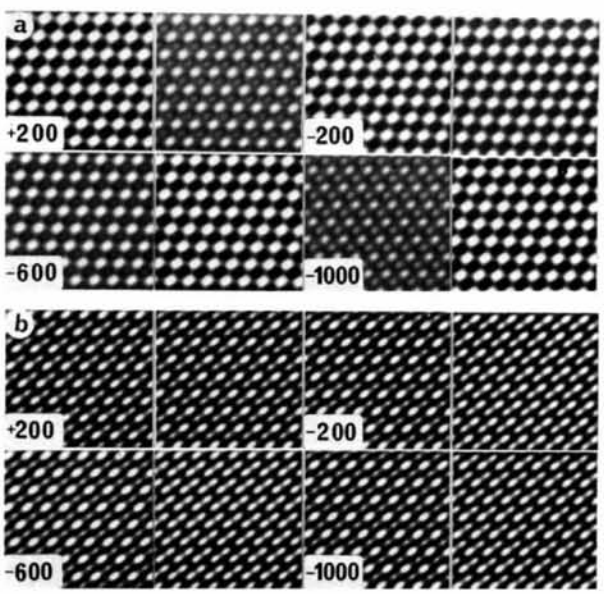

Fig. 10. Through-focal series (200 Å steps) of 3*C* images at 500 kV. (*a*) 30·7 Å thick; (*b*) 153 Å thick. C_s = 3·5 mm; α = 0·3 mrad; Δ = 250 Å; aperture cut-off 2·5 Å.

ticularly those containing defects which scatter over a wide range of spatial frequencies, should not proceed until the imaging conditions (*i.e.* C_s, α and Δ) are first established, and appropriate simulations carried out.

4. Discussion

Our immediate concern has been to establish, using image simulation, the possibilities for direct structure imaging of silicon carbide in the high-resolution electron microscope with the pre-requisite of realistic operating conditions. This restriction conveniently limits the combinations of microscope and crystal parameters which might otherwise need to be considered; however, our simulations are still sufficiently representative for some useful generalizations to be made.

It is interesting that calculations of the WPO image as a function of aperture cut-off indicate that resolutions of close to 1 Å are required before splitting of 'atom pairs' (projected separation of 1·09 Å) into individual spots *at the atomic positions* starts to occur, and considerably better than 1 Å is needed before differences in intensity of the individual Si and C atoms are clearly apparent. The achievement of a value for δ, the directly interpretable image resolution, of 1 Å is well beyond the capabilities of any existing electron microscope: at 1 MV, this resolution requires a spherical-aberration coefficient of 0·75 mm, which exceeds the limits of what might be achieved even with a highly saturated objective lens at this voltage (Cleaver, 1981). It will clearly also be extremely difficult to resolve the separate atom pairs in both Si and Ge in the (110) projection, where the spacing is 'only' ~1·4 Å. Comparison with our simulations for silicon carbide, which has a very similar geometry, would suggest the need for a WPO resolution of better than 1·4 Å, and hence for δ to be around 1·2 Å.

Imaging of the individual tetrahedra of silicon carbide in the high-voltage HREM, in particular to identify polytypic stacking sequences, appears superficially straightforward, given the tetrahedral-layer separation of 2·5 Å. However, despite a resolution limit approaching 2 Å in most of the above simulations, it is evident that the tetrahedral stacking will only be directly recognizable under very restricted imaging conditions and for quite thin crystals (typically around 75 Å at most). Thereafter, non-linear effects render images increasingly less interpretable even though patterns reminiscent of the projected atomic and tetrahedral structure sometimes occur. Note that it may still be possible to recover the linear image for intermediate thicknesses using pairs of images taken at maximum and minimum contrast (O'Keefe & Sanders, 1976), or, indeed, to get back to the specimen structure (in projection) from bright- and dark-field images (Saxton, 1981). However, in thicker specimens there is increasing divergence between experimental micrographs and theoretical simulations (*e.g.* Smith, Jefferson & Mallinson, 1981), and some adequate means for incorporating inelastic scattering into the image simulations needs to be developed in order initially to close this gap and, eventually, to enable some sort of inversion whereby experimental micrographs might be correctly interpreted. This is obviously much more serious in the presence of crystal defects of unknown structure – it then becomes necessary to rely on simulations of any neighbouring perfect material so that at least the imaging conditions (*i.e.* C_s, α and Δ) are well characterized (Wilson, Spargo & Smith, 1982).

Finally, it is relevant to point out that these calculations have been performed with the convenient assumption of optimal specimen and microscope characteristics, particularly cleanliness and crystal orientation. Real specimens of silicon carbide are likely to be covered with some amorphous surface layer, perhaps arising from the preparation technique and possibly also from contamination inside the microscope, which will degrade contrast levels, and hence resolution. Moreover, whilst it is well appreciated that high-resolution structure images are sensitive to crystal tilt, it has also been recently shown that the alignment of the incident illumination can be even more critical (Saxton & O'Keefe, 1981; Smith, Saxton, Stobbs, Wood & O'Keefe, 1983). These further experimental factors need to be accounted for in any quantitative investigation involving comparisons between experimental micrographs and simulated images.

Financial support from the Science and Engineering Research Council, England, is gratefully acknowledged.

References

ALLPRESS, J. G. & SANDERS, J. V. (1973). *J. Appl. Cryst.* **6**, 165–190.
BURSILL, L. A. & WOOD, G. J. (1978). *Philos. Mag.* **38**, 673–689.
CLEAVER, J. R. A. (1981). *Optik*, **58**, 409–432.
COSSLETT, V. E., CAMPS, R. A. SAXTON, W. O., SMITH, D. J., NIXON, W. C., AHMED, H., CATTO, C. J. D., CLEAVER, J. R. A., SMITH, K. C. A., TIMBS, A. E., TURNER, P. W. & ROSS, P. M. (1979). *Nature (London)*, **281**, 49–51.
COWLEY, J. M. (1975). *Diffraction Physics*. Amsterdam: North-Holland.
COWLEY, J. M. & MOODIE, A. F. (1957*a*). *Acta Cryst.* **10**, 609–619.
COWLEY, J. M. & MOODIE, A. F. (1957*b*). *Proc. Phys. Soc. London*, **70**, 486–496.
ERIKSON, P. H. & KLUG, A. (1971). *Philos. Trans. R. Soc. London Ser. B*, **261**, 105–118.
FIELDS, P. M. & COWLEY, J. M. (1978). *Acta Cryst.* A**34**, 103–112.
HASHIMOTO. H., ENDOH, H., TAKAI, Y., TOMIOKA, H. & YOKOTA, Y. (1978/79). *Chem. Scr.* **14**, 23–31.
HIRABAYASHI, M. (1980). *Electron Microscopy* 1980. Vol. 4. *High Voltage*, edited by P. BREDEROO & J. VAN LANDUYT, pp. 142–149. Leiden: Seventh European Congress on Electron Microscopy Foundation.
HORIUCHI, S., MATSUI, Y., BANDO, Y., KATSUTA, T. & MATSUI, I. (1978). *J. Electron Microsc.* **27**, 39–46.

HUTCHISON, J. L., ANSTIS, G. R., HUMPHREYS, C. J. & OURMAZD, A. (1981). *Electron Microscopy and Analysis*, 1981, edited by M. J. GORINGE, pp. 357–360. Bristol and London: Institute of Physics.
IIJIMA, S. & O'KEEFE, M. A. (1979). *J. Microsc. (Oxford)*, **117**, 347–354.
IZUI, K., FURUNO, S., NISHIDA, T. & OTSU, H. (1978/79). *Chem. Scr.* **14**, 98–108.
JEPPS, N. W. & PAGE, T. F. (1979). *J. Microsc. (Oxford)*, **116**, 159–171.
JEPPS, N. W. & PAGE, T. F. (1980). *J. Microsc. (Oxford)*, **119**, 177–188.
JEPPS, N. W., SMITH, D. J. & PAGE, T. F. (1979). *Acta Cryst.* A**35**, 916–923.
KOBAYASHI, K., SUITO, E., UYEDA, N., WATANABE, M., YANAKA, T., ETOH, T., WATANABE, H. & MORIGUCHI, M. (1974). *Electron Microscopy* 1974, Vol. 1, edited by J. V. SANDERS & D. J. GOODCHILD, pp. 30–31. Canberra: Australian Academy of Science.
KRIVANEK, O. L. & REZ, P. (1980). *Proc. 38th Ann. Meet. EMSA*, edited by G. W. BAILEY, pp. 170–171. Baton Rouge: Claitor's.
O'KEEFE, M. A. (1979). *Proc. 37th Ann. Meet. EMSA*, edited by G. W. BAILEY, pp. 556–557. Baton Rouge: Claitor's.
O'KEEFE, M. A. & BUSECK, P. R. (1979). *Trans. Am. Crystallogr. Assoc.* **15**, 27–46.
O'KEEFE, M. A., BUSECK, P. R. & IIJIMA, S. (1978). *Nature (London)*, **274**, 322–324.
O'KEEFE, M. A., JEPPS, N. W., STOBBS, W. M. & SMITH, D. J. (1983). In preparation.
O'KEEFE, M. A. & PITT, A. J. (1980). *Electron Microscopy* 1980. Vol. 1. *Physics*, edited by P. BREDEROO & G. BOOM, pp. 122–123. Leiden: Seventh European Congress on Electron Microscopy Foundation.
O'KEEFE, M. A. & SANDERS, J. V. (1976). *Optik*, **46**, 421–430.
SAXTON, W. O. (1981). *J. Microsc. Spectrosc. Electron.* **15**, 661–670.
SAXTON, W. O. & O'KEEFE, M. A. (1981). *Electron Microscopy and Analysis*, 1982, edited by M. J. GORINGE, pp. 343–346. Bristol and London: Institute of Physics.
SHAFFER, P. T. B. (1969). *Acta Cryst.* B**25**, 477–488.
SMITH, D. J., CAMPS, R. A. & FREEMAN, L. A. (1981). *Electron Microscopy and Analysis*, 1981, edited by M. J. GORINGE, pp. 381–386. Bristol and London: Institute of Physics.
SMITH, D. J., JEFFERSON, D. A. & MALLINSON, L. A. (1981). *Acta Cryst.* A**37**, 273–280.
SMITH, D. J., JEPPS, N. W. & PAGE, T. F. (1978). *J. Microsc. (Oxford)*, **114**, 1–18.
SMITH, D. J., SAXTON, W. O., STOBBS, W. M., WOOD, G. J. & O'KEEFE, M. A. (1983). *Ultramicroscopy*. Submitted.
SPENCE, J. C. H., O'KEEFE, M. A. & KOLAR, H. (1977). *Optik*, **49**, 307–323.
VERMA, A. R. & KRISHNA, P. (1966). *Polymorphism and Polytypism in Crystals*. New York: John Wiley.
WILSON, A. R. (1980). *Micron*, **11**, 281–283.
WILSON, A. R., BURSILL, L. A. & SPARGO, A. E. (1978/79). *Optik*, **52**, 313–336.
WILSON, A. R., SPARGO, A. E. & SMITH, D. J. (1982). *Optik*, **61**, 63–79.

Acta Cryst. (1983). A**39**, 148–158

Statistical Description of Multimodal Atomic Probability Densities

BY W. F. KUHS

Institut Laue–Langevin, 156X Centre de Tri, 38042 Grenoble CEDEX, France

(*Received* 10 *June* 1982; *accepted* 6 *September* 1982)

Abstract

A general method for describing multimodal atomic densities is presented. It is based on series expansions of a harmonic Gaussian probability density function. The most suitable expansion is of the Gram–Charlier type; its Fourier transform can be easily inserted in a structure factor equation. This statistical method yields a satisfactory fit to the data and allows for a better interpretation of the fit parameters than sophisticated split-atom models. The method is especially useful for weakly resolved modes and allows a better distinction between disorder and anharmonic motion than in conventional Fourier syntheses. Calculations on $CsPbCl_3$, ice I*h* and $RbAg_4I_5$ are presented to show the strengths and the limitations of this method.

1. Introduction

Disordered solids with low transition barriers can be described crystallographically in two fundamentally different ways: (*a*) using split-atom models ('split models') with partial occupancies or (*b*) using anharmonic probability density functions (p.d.f.'s) with full occupancies and more than one local maximum of density ('multimodality'). Only the latter method yields directly physically meaningful model parameters owing to the lack of intersite correlations. It allows a straightforward evaluation of the p.d.f. in the overlap region of the split atoms. The evaluation of the true p.d.f. around the transition barrier is of great importance, *e.g.* in structures of ionic conductors or in hydrogen-bonding situations, and it is in the end indispensable for distinguishing true disorder from pronounced thermal motion.

A generalized model p.d.f. is clearly needed for modelling such a possibly multimodal atomic p.d.f. This general p.d.f. must fulfil the following conditions: (*a*) parametrizability and Fourier transformability to allow inclusion in a least-squares refinement procedure; (*b*) compatibility with symmetry requirements to allow

0567-7394/83/010148-11$01.50